ISSN: 0067-2904
GIF: 0.851

Simulation of Solar Coronal Magnetic Field Using Potential Field Model

Loay K. Abood[1]*, Kamal M. Abood[2], Huda S. Ali[2]
[1]Department of Computer Science, College of Science, University of Baghdad, Baghdad, Iraq
[2]Department of Astronomy and Space Science, College of Science, University of Baghdad, Baghdad, Iraq

Abstract

In this paper, 3D simulation of the global coronal magnetic field, which use observed line of sight component of the photosphere magnetic field from (MDI/SOHO) was carried out using potential field model. The obtained results, improved the theoretical models of the coronal magnetic field, which represent a suitable lower boundary conditions (B_x , B_y , B_z) at the base of the linear force-free and nonlinear force free models, provides a less computationally expensive method than other models. Generally, very high speed computer and special configuration is needed to solve such problem as well as the problem of viewing the streamline of the magnetic field. For high accuracy special mathematical treatment was adopted to solve the computation complexity.

Keywords: solar coronal, magnetic field, potential field, magnetogram.

محاكاة المجال المغناطيسي للأكليل الشمسي بأستخدام نموذج المجال الكامن

لؤي كاظم عبود[1]*، كمال محمد عبود[2] ,هدى شاكر علي[2]
[1]قسم علوم الحاسبات، كلية العلوم، جامعة بغداد، بغداد، العراق
[2]قسم علوم الفلك والفضاء، كلية العلوم، جامعة بغداد، بغداد، العراق

الخلاصة

في هذا البحث تم محاكاة نموذج ثلاثي الابعاد للمجال المغناطيسي للاكليل الشمسي، بأستخدام مركبة خط البصر المرصود للمجال المغناطيسي للطبقة المرئية الشمسية من (MDI/SOHO)، بأستخدام تقنية المجال الكامن. النتائج المحصلة حسنت عمل النماذج النظرية للاكليل الشمسي، و هذه النتائج تمثل الشروط الحدودية الدنيا (B_x , B_y , B_z) لقاعدة نموذج القوة الخطية الحرة والقوة غير الخطية الحرة، وتوفر طريقة حسابية أسهل من النماذج الأخرى. عموما، هناك حاجة كبيرة لكمبيوتر سريع جدا ذو مواصفات خاصة لحل مثل هذه المشكلة فضلا عن مشكلة عرض خطوط المجال المغناطيسي. لغرض الدقة العالية تم تبني معالجة رياضية خاصة لحل التعقيدات الرياضية.

1. Introduction

The Potential-field Source-surface (PFSS) model provides a simple and effective model for the large-scale features of the global coronal magnetic field. To capture large-scale field structure in a model we may assume that the electric currents in the corona do not significantly influence the global field structure. The (PFSS) model was originally developed by (Schatten, Wilcox & Ness (1969) and refined by (Hoeksema (1984), Wang & Sheeley (1992) and (Wang & Sheeley, 2002). The PFSS model gives a reasonable estimate of the coronal field structure because most of the coronal field is approximately Maxwell-stress-free most of the time (Neugebauer et al. 2006, Riley et al. 2012) [1]. In this paper, used potential field source surface (PFSS) technique that have been developed to model the

*Email: hudashaker@yahoo.com

coronal magnetic field based on the input of photospheric magnetic fields. This study is the inference of the true 3D magnetic field geometry, which can be accurately measured by Michelson Doppler Imager (MDI) with the dual spacecraft Solar and Heliospheric Observatory (SOHO), and thus it provides a most crucial input to test theoretical magnetic field models.

2. Potential field source surface model

Potential Field Source Surface (PFSS) Model provide an approximate description of the solar coronal magnetic field based on observed photospheric fields (magnetograms). The equations for the magnetic field in this model are [2]:

$$\nabla \times \mathrm{B} = 0 \tag{1}$$

And

$$\nabla . \mathrm{B} = 0 \tag{2}$$

Where B is magnetic field, and ∇ represents gradient.

The simplest representation of a magnetic potential field that fulfills Maxwell divergence-free condition *($\nabla \cdot B = 0$)* is a magnetic charge that is buried below the solar surface (to avoid magnetic monopoles in the corona), which predicts a magnetic field $B(x)$ that points away from the buried unipolar charge and whose field strength falls off with the square of the distance r [3],

$$B(x) = B_o \left(\frac{d_o}{r}\right)^2 \frac{\boldsymbol{r}}{r} \tag{3}$$

Where B_o is the magnetic field strength at the solar surface directly above the buried magnetic charge, $\boldsymbol{r_o} = (x_o, y_o, z_o)$ is the subphotospheric position of the buried charge, $d_o = \sqrt{1 - x_o^2 - y_o^2 - z_o^2}$ is the depth of the magnetic charge, and $\boldsymbol{r} = [(x - x_o), (y - y_o), (z - z_o)]$ is the solar corona from the location $\boldsymbol{r_o}$ of the buried charge [4].

In order to obtain the Cartesian coordinates (B_x, B_y, B_z) of the magnetic field vector $B_j(x)$, (the distance from the magnetic charge j) can rewrite equation (3) as [5],

$$B_x(x, y, z) = B_0 \left(\frac{d_0}{r}\right)^2 \frac{(x - x_0)}{r} \tag{4}$$

$$B_y(x, y, z) = B_0 \left(\frac{d_0}{r}\right)^2 \frac{(y - y_0)}{r} \tag{5}$$

$$B_z(x, y, z) = B_0 \left(\frac{d_0}{r}\right)^2 \frac{(z - z_0)}{r} \tag{6}$$

For arbitrary line-of-sight magnetogram with a superposition of N_m magnetic charges, so that the potential field can be represented by the superposition of Nm fields B_j from each magnetic charge $j = 1, \ldots, N_m$ [5],

$$B(x) = \sum_{j=1}^{N_m} B_j(x) = \sum_{j=1}^{N_m} B_j \left(\frac{d_j}{r}\right)^2 \frac{\boldsymbol{r}}{r} \tag{7}$$

With $\boldsymbol{r} = [(x - x_j), (y - y_j), (z - z_j)]$ the distance from the magnetic charge j. Since the divergence operator is linear, the superposition of a number of potential field is divergence-free also [6]

$$\nabla . B = \nabla . \left(\sum_j B_j\right) = \sum_j (\nabla . B_j) = 0 \tag{8}$$

This way can parameterize a 3D magnetic field *B(x)*. The formal boundary conditions for the potential model are the prescription of the normal component of the magnetic field at the photosphere. Observations determine the line-of-sight component of the magnetic field more accurately than the transverse component, and early instruments provided only the line-of-sight component. An equivalent formulation of the boundary value problem based on a prescription of *B* at the photosphere is more useful in practice [7].

3. Three Dimensions Geometry of the Solar Surface

To determine an approximate 3D magnetic field model of a solar active region, using a magnetogram that contains the line-of-sight magnetic field component. Started with the absolute peak in the magnetogram, a 3D parameterization of line of sight (LOS) magnetogram $B_z(x, y)$ can be

obtained by a superposition of buried magnetic point charges, which produce a surface magnetic field $B = (B_x, B_y, B_z)$ that is constrained by the observed magnetogram [8].

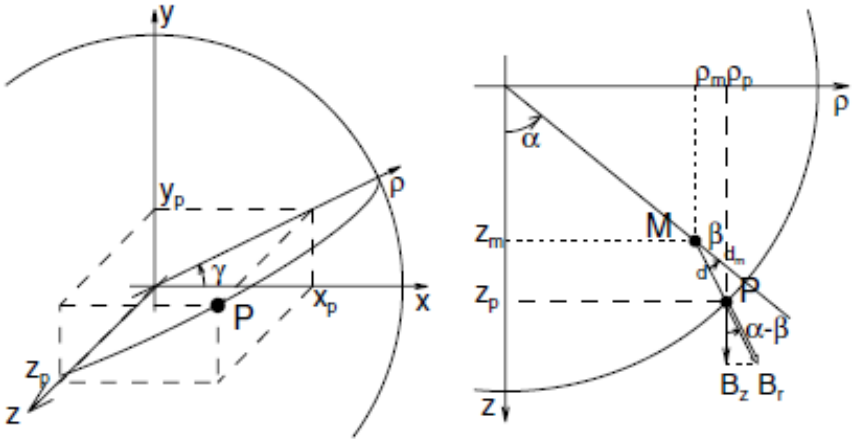

Figure 1-3D geometry of a point source $P = (x_p, y_p, z_p)$ in a Cartesian coordinate system is shown (left). The geometry of a line-of-sight magnetic field component B_z is shown in the (z, ρ)-plane on the right-hand side [9].

And describe the geometric inversion of the 3D coordinates (x_m, y_m, z_m) and surface field strength B_m of a single magnetic point charge M that produces a local peak B_z with width w at an observed position (x_p, y_p),Figure-1. The geometric relationships can be derived most simply in a plane that intersects the point source P and the line-of-sight axis. In the plane of sky, and define a coordinate axis **ρ** that is orthogonal to the line-of-sight axis **z**, and is rotated by an angle **γ** with respect to the *x-axis*, so that we have the transformation [9, 10]:

$$\rho_p = \sqrt{x_p^2 + y_p^2} \tag{9}$$

$$x_p = \rho_p \cos(\gamma) \tag{10}$$

$$y_p = \rho_p \sin(\gamma) \tag{11}$$

$$z_p = \sqrt{1 - \rho_p^2} \tag{12}$$

$$\alpha \approx \arctan\left({}^{\rho_p}/_{z_p}\right) \tag{13}$$

$$\gamma = \arctan\left({}^{y_p}/_{x_p}\right) \tag{14}$$

$$\beta_p = atctan\left[\frac{\sqrt{9 + 8tan^2\alpha} - 3}{4} tan\ \alpha\right] \tag{15}$$

$$B_m = \frac{B_z}{\left[cos^2\beta_p \cos(\alpha - \beta_p)\right]} \tag{16}$$

$$\beta_2 = \arccos\left[((cos\beta_p)^3/2)^{1/3}\right] \tag{17}$$

$$d_m = \frac{w}{[tan\beta_2\ cos\alpha(1 - 0.1\alpha)]} \tag{18}$$

$$r_m = (1 - d_m) \tag{19}$$

$$\rho_m = \frac{\rho_p - d_m \sin(\alpha - \beta_p)}{cos\beta_p} \tag{20}$$

$$z_m = \sqrt{r_m^2 - \rho_m^2} \tag{21}$$

$$x_m = \rho_m \cos(\gamma) \tag{22}$$

$$y_m = \rho_m \sin(\gamma) \tag{23}$$

While the half-width w was [11]:

$$w = \rho_2 - \rho_p = d_m \left[\frac{\sin(\alpha - \beta_2)}{\cos \beta_2} - \frac{\sin(\alpha - \beta_p)}{\cos \beta_p} \right] \quad (24)$$

Which are found in Gaussian 2D distribution functions. Now, they have all the geometric relationships to invert the theoretical parameters (B_m, x_m, y_m, z_m) from the observables $(B_z, \rho_p, z_p, \omega)$. In this algorithm, iteratively determine the local peaks of the (LOS) components $B_z(x, y)$ and their widths w, and invert the model parameters (B_m, x_m, y_m, z_m) with the inversion procedure given in equations (9-24). From the observables (B_z, x_p, y_p) and the calculated d_m for the depth of the buried magnetic charge. Else, calculated the projected disk center distance ρ_p, the LOS coordinate z_p at the photospheric height, the angle α between the LOS and solar surface vertical, the angle β_p between the solar surface vertical and the LOS field component B_z, which yield then the field strength B_m and the coordinates $(x_m, y_m, z_m, r_m, \rho_m)$ of the buried magnetic charge M[12,13].

4. Algorithm and Results and Discussion

The developed model can be used to calculate the magnetic field distribution of the sun's surface in 3D. The proposed model can be summarized as follows:

1. Read (LOS) of magnetogram.
2. Extract positive magnetic region.
3. Select peak value of magnetic field.
4. Open window about this value location.
5. Fit the extracted field from step above by 2D Gauss fit to determine center, amplitude and full width of half maximum (FWHM) value.
6. Apply equations (9-24) to get (x_m, y_m, z_m, B_m).
7. Delete the selected window from the original extracted region from step 1.
8. Iteratively repeat steps (2-7) until all points are used.
9. Repeat all steps for negative magnetic field region.
10. After extracting the needed features of the solar magnetogram, apply equation (4-6) to calculate (B_x, B_y, B_z) at each specified location.

The three different modules of the algorithm can be organized into three groups: Input module (1), forward-fitting modules (2), and output module (3), which described in the following:

1.1 Observational Input: This module inputs external data directly, such as (LOS) magnetograms $B_r(x, y)$ from a recent (MDI) magnetogram, where the MDI to study the evolution of active regions with its high cadence (96s), continuous time coverage, and good spatial resolution($2^{"}$ $pixel$)). From the LOS data N_m of magnetic field points will be selected due to intensity to derive the magnetic field parameter like position (x_j, y_j, z_j) and magnetic strength utilizing buried charge theory. Figures-2 and 3 shows MDI/SOHO image and active region that was chosen.

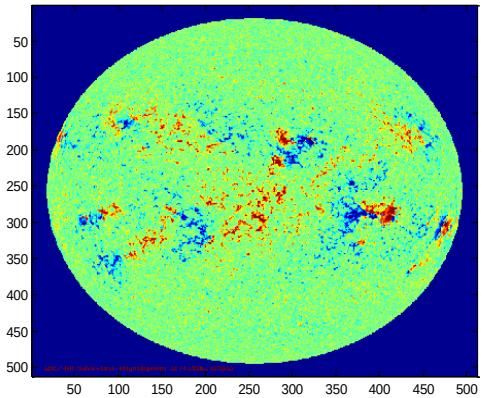

Figure 2- MDI/SOHO image.

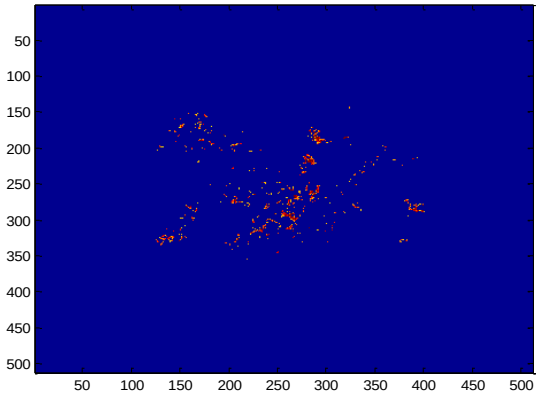

Figure 3- Active Region which chosen.

4.2 Forward-Fitting of Potential-Field Parameters: Decomposing the (LOS) magnetogram into a N_m number of buried magnetic charges that reflect a 2D Gaussian-like distribution in the magnetogram. This decomposition is carried by iteratively select maximum field strength points. A rectangular window centering round the selected maximum points to extract the field parameters (x_j, y_j, z_j, B_j), j = 1, . . . , N_m, then 3D potential field is obtained that fulfill maxwell's divergence- free equations (1) and (2). Figures-4 and 5, present the main results of Potential Field model simulation of B_z, in 3D and 2D, respectively. And Figures-6 and 7, show streamlines of the Potential Field Model simulation of B_z in 3D and 2D.

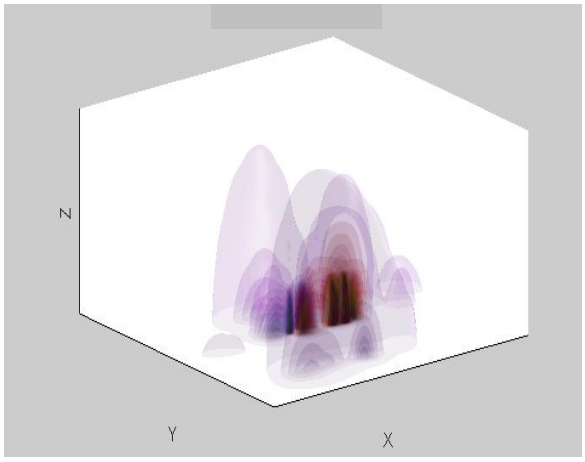

Figure 4- Simulations of potential field,

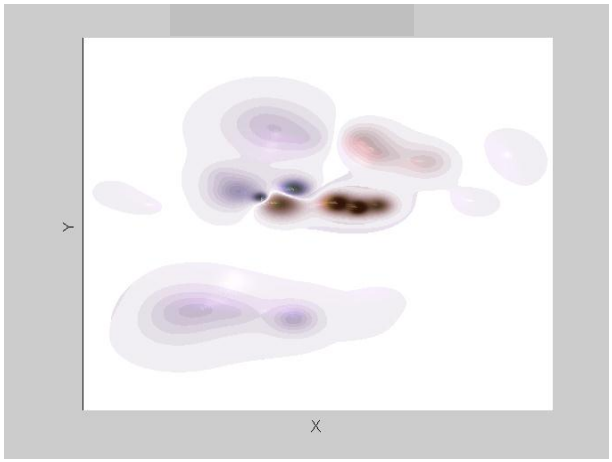

Figure 5- Simulations of potential field

In this work, twenty layers were used to represent the high from the sun surface of the computational domain. The values on the lower surface are determined from observational data. Thus this surface is referred to as the source surface, i.e., the photosphere. Values on the other surface are prescribed according to both physical and mathematical continuity conditions. Figures (8-10) show the predicts of the transverse field components $B_x(x, y, z_{ph})$and $B_y(x, y, z_{ph})$ from the (LOS) magnetogram $B_r(x, y, z_{ph})$, where is z_{ph} the photospheric surface level $(1\ to\ 20\ level)$.

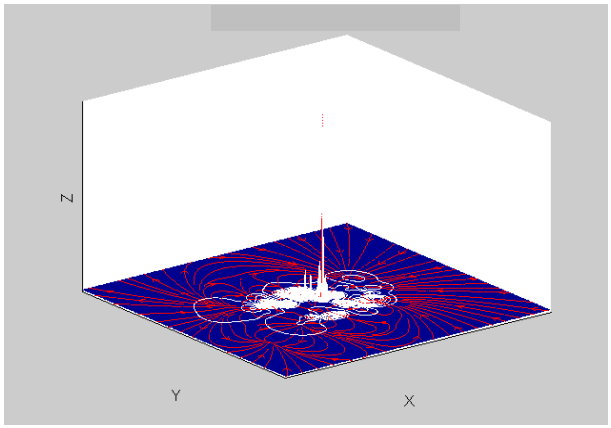

Figure 6- Simulations of potential field, in 3D.

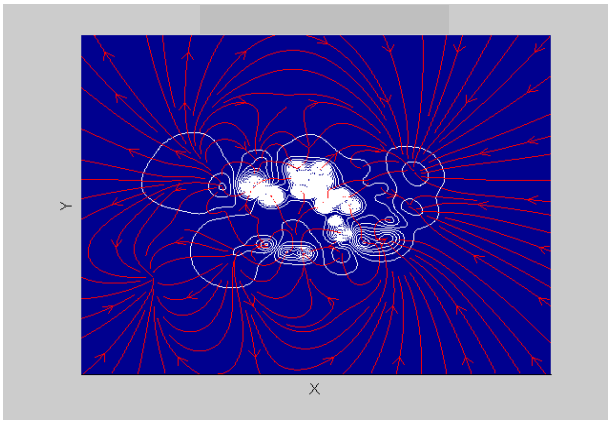

Figure 7- Simulations of potential field, in 2D.

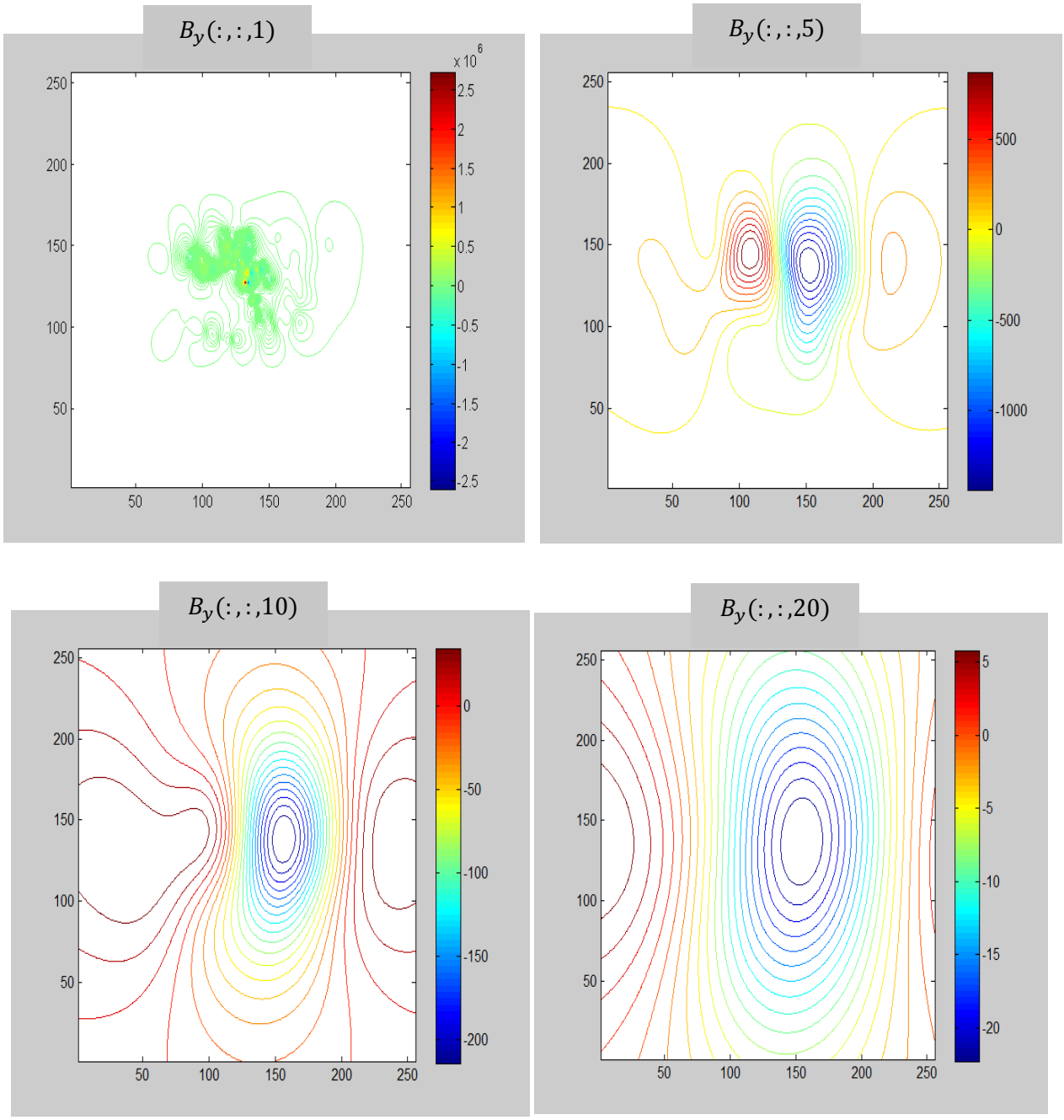

Figure 9- $B_y(x, y, z_{ph})$ with the photospheric level at z_{ph}

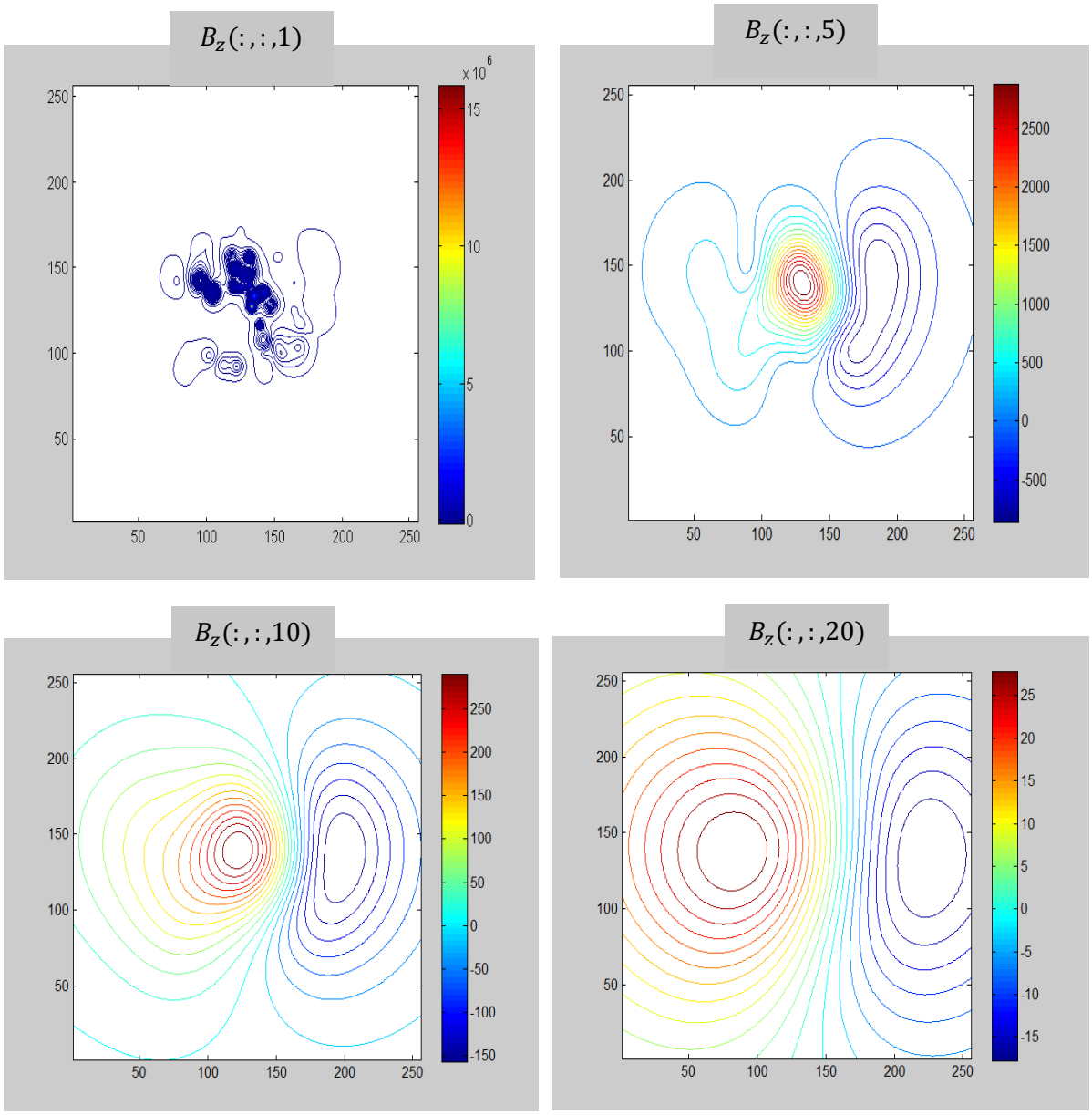

Figure 10- $B_z(x, y, z_{ph})$ with the photospheric level at z_{ph}

4.3 Display of 3D Projections*:* in order to draw the total magnetic field from the three magnetic components$B_x(x, y, z)$, $B_y(x, y, z)$ and $B_z(x, y, z)$. We need a special program for representation. This program called paraveiw, which is an open source tookl kit plat form for 3D computer graphics and visualization. It can be free downloaded from the website (http://www.paraview.org/download/). Figures-11 and 12 show the magnetic field streamlines of PFSS.

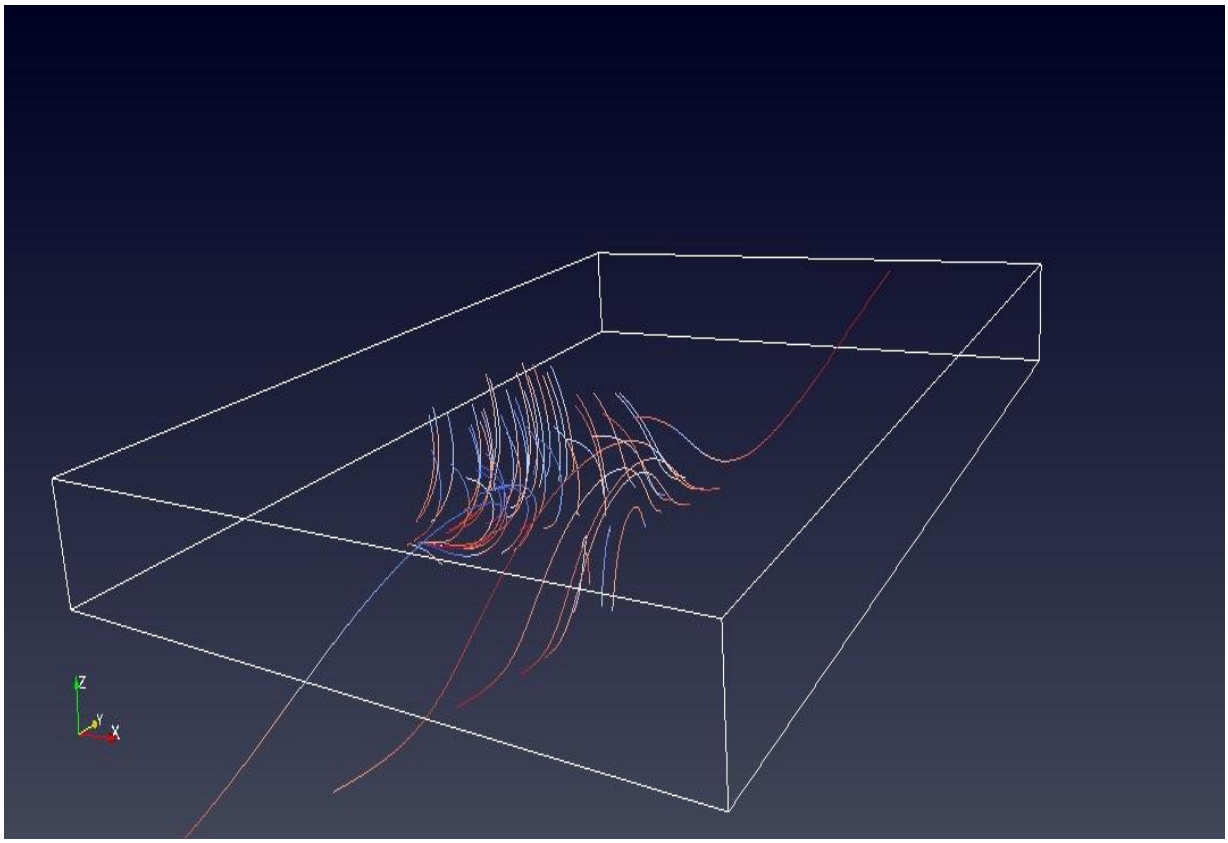

Figure 11- Magnetic Field lines in PFSS Model, in (zx) side view.

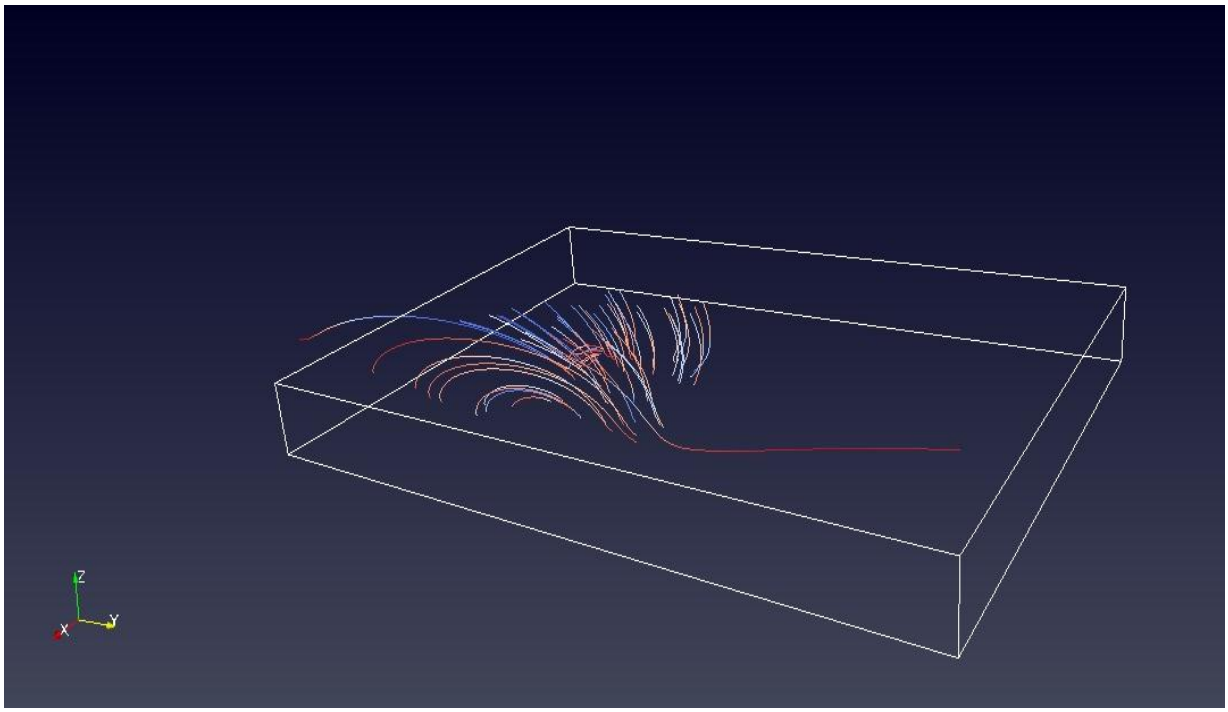

Figure 12- Magnetic Field lines in PFSS Model, in (zy) side view.

Conclusions

The main conclusion could be summarized by the following points:

1. The extrapolation algorithms are very computing-intensive, because a good solution requires many iterations on a large computational 3D-grid that has sufficient spatial resolution to resolve the relevant magnetic field gradients. The fastest computational way would be an explicit analytical solution for the coronal field vectors $B(r)$ as a function of some suitable parameterization of the boundary data or coronal constraints, a fast computation algorithm that can perform many interactions without computing intensive techniques.
2. A line-of-sight magnetogram that measures the longitudinal magnetic field component $B_z(x,y)$ can be decomposed into $N_m \approx 150$ for example magnetic charges, from which maps of all three magnetic field components $B_x(x,y)$, $B_y(x,y)$, and $B_z(x,y)$ can be reconstructed at the solar surface.
3. The application of MDI/SOHO line-of-sight magnetograms constrained model allows us to obtain maps of the non-potential magnetic field components, $B_x(x,y)$, $B_y(x,y)$, and $B_z(x,y)$.

References

1. Mikic´, D. H. and Yeates, A. R. **2012**. The Sun's Global Photospheric and Coronal Magnetic Fields: Observations and Models. *Living Reviews in Solar Physics*, 9(6), pp: 9-21.
2. Guo, Y., Ding, M. D., Liu, Y., Sun, X. D., DeRosa, M. L., and Wiegelmann, T. **2012**. Modeling Magnetic Field Structure of a Solar Active Region Corona Using Nonlinear Force-free Fields in Spherical Geometry. *The Astrophysical Journal*, 760(1), pp: 47-61.
3. Aschwanden, M. J., Wuelser, J. P., Nitta, N. V., Lemen, J. R., DeRosa, M. L., and Malanushenko, A. **2012**. First Three-dimensional Reconstructions of Coronal Loops with the STEREO A+B Spacecraft. IV. Magnetic Modeling with Twisted Force-free Fields. *The Astrophysical Journal*, 756(2), pp: 124-146.
4. Wang, Y.-M., and Sheeley, N. R. **1992**. On potential field models of the solar corona. *The Astrophysical Journal*, 392(1), pp: 310-319.
5. Aschwanden, M. J. **2013**. A Nonlinear Force-Free Magnetic Field Approximation Suitable for Fast Forward-Fitting to Coronal Loops. I. Theory. *Solar Physics*, 287(1-2), pp: 323-344.
6. Riley, P., Linker, J. A., Mikic, Z., Lionello, R., Ledvina, S. A., and Luhmann, J. G. **2006**. A Comparison between Global Solar Magnetohydrodynamic and Potential Field Source Surface Model Results. *The Astrophysical Journal*, 653(2), pp: 1510-1516.
7. ČADÉZ, V. M. et al. **2005**. Theoretical Modeling of Potential Magnetic Field Distribution in the Corona above Axially Symmetric Photospheric Active Regions in a Uniform Magnetic Field. *Astrophysics and Space Science Library*, 320, pp: 279-282.
8. Tadesse, T., Wiegelmann, T., Olson, K., and MacNeice, P. J. **2013**. Modeling coronal magnetic field using spherical geometry: cases with several active regions. *Astrophysics and Space Science*, 347(1), pp: 21-27.
9. Aschwanden, M. J., Xu, Y., and Jing, J. **2014**. Global Energetics of Solar Flares. I. Magnetic Energies. *Astrophysical Journal*, 797(1), pp: 50-85.
10. Aschwanden, M. J., Wuelser, J. P., Nitta, N. V., Lemen, J. R., DeRosa, M. L., and Malanushenko, A. **2012**. First 3D Reconstructions of Coronal Loops with the STEREO A+B Spacecraft: IV. Magnetic Modeling with Twisted Force-Free Fields. *The Astrophysical Journal*, 756(1), pp: 124-146.
11. Aschwanden, M. J., Wülser, J. P., Nitta, N. V., and Lemen, J. R. **2008**. First Three-Dimensional Reconstructions of Coronal Loops with the STEREO A and B Spacecraft. I. Geometry. *The Astrophysical Journal*, 679(1), pp: 827-842.
12. Bobra, M. G.; van Ballegooijen, A. A.; DeLuca, E. E. **2008**. Modeling Nonpotential Magnetic Fields in Solar Active Regions. *The Astrophysical Journal*, 672(2), pp: 1209-1220.
13. Low, B. C. **1985**. Three-dimensional structures of magnetostatic atmospheres. I - Theory. *The Astrophysical Journal*, 293(1), pp: 31-43.